energy&fuels

pubs.acs.org/EF

Article

Ultrafast Exciton Dynamics in Thin Films of a Two-Dimensional Pb-Free $CsBi_3I_{10}$ Perovskite

Published as part of Energy & Fuels special issue "2025 Pioneers in Energy Research: Prashant Kamat".

Kai-Chun Chou, David C. Zeitz, Mariam Khvichia, Jeremy L. Barnett, and Jin Z. Zhang*

Cite This: *Energy Fuels* 2024, 38, 21382–21387

Read Online

ACCESS | Metrics & More | Article Recommendations | Supporting Information

ABSTRACT: $CsBi_3I_{10}$ perovskite films were synthesized by an antisolvent-assisted spin-coating method. The morphology and crystal structure of the $CsBi_3I_{10}$ perovskite film were characterized using scanning electron microscopy (SEM), X-ray diffraction (XRD), and Raman spectroscopy, confirming its crystallinity and purity. Ultraviolet–visible (UV–vis) absorption spectra revealed two excitonic peaks peaked at 496 and 626 nm. Femtosecond transient absorption spectroscopy (TAS) was utilized to probe the exciton dynamics that reveal three dominant processes attributed to hot electron cooling, trapping to trap states, electron–hole recombination, and a possible dissociative pathway or high density of defect states coupled with the first excited electronic state or conduction band (CB), which lead an overall short-lived photoinduced charge carrier or exciton. A kinetic model was proposed to simulate and explain these processes that lead to an overall short exciton lifetime.

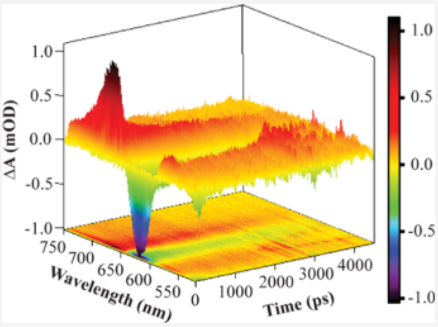

Lead halide perovskites (LHPs) have emerged as a class of materials with promising optoelectronic properties and potential applications in photodetectors, solar cells, light-emitting diodes (LEDs), optical fibers, and lasers, among others.[1−6] Despite their promising performance, the inherent toxicity of lead and issues related to long-term stability pose significant environmental and health concerns, limiting their widespread application in photovoltaic (PV) and optoelectronic devices.[7] Consequently, developing non-toxic and stable Pb-free perovskite alternatives has become a critical research focus.[8] Elements that can substitute Pb have been identified as those that exhibit similar physical properties to Pb and include Bi,[9,10] Sn,[11,12] Ge,[13,14] and Cu.[15,16] Bi and Pb are adjacent elements in the same period, with Bi^{3+} having a similar ionic radius and $6s^26p^0$ electronic configuration as Pb^{2+}, and thus, similar optoelectronic properties can be expected when it is incorporated into the perovskite lattice. Bi-based halide perovskites have been shown to retain the desirable optoelectronic properties of their lead counterparts while offering enhanced environmental safety and stability.[17−20] These materials exhibit a large absorption coefficient and a wide spectral detection range,[17] making them attractive candidates for various optoelectronic applications.

Bi-based halide perovskites, such as $A_3Bi_2X_9$,[19] ABi_3X_{10},[21] and double perovskite $A_2B^+Bi^{3+}X_6$,[8] have emerged as a promising class of photovoltaic materials because of their reduced toxicity, rich structural diversity, and optoelectronic properties.[22,24,25] Among all reported Bi-based light absorber materials, $CsBi_3I_{10}$ has attracted increasing attention due to its intriguing properties, such as a small bandgap (1.77 eV), large absorption coefficient (1.4×10^5 cm^{-1}), and long-term stability.[26,27] However, despite these promising features, the power conversion efficiencies (PCEs) of Bi-based perovskites, such as $Cs_3Bi_2I_9$, $CsBi_3I_{10}$, and $Cs_2AgBiBr_6$, remain significantly lower than their theoretical potential, with reported PCEs of only 1.09,[28] 2.3,[29] and 2.51%,[30] respectively. Although various strategies have been employed to enhance their photovoltaic performance, these efforts are hampered by a lack of a fundamental understanding of the intrinsic physical properties of pristine Bi-based perovskites.

To fully explore bismuth halide perovskites' potential in photovoltaic devices, a detailed understanding of their photoexcited states is critical. However, for lead-free Bi halide perovskites, only a few reports regarding their photoexcited-state dynamics are available. For example, Tailor et al. utilized ultrafast spectroscopy to show that hot carrier cooling rates in $A_3Bi_2I_9$ perovskites depend upon the A cation (FA^+, MA^+, and Cs^+), with Cs^+ facilitating the fastest cooling, which has implications for optimizing exciton behavior in photovoltaic devices.[23] Scholz et al. examined the exciton dynamics in $MA_3Bi_2I_9$ films on mesoporous TiO_2, revealing that the interaction with the scaffold significantly enhances exciton

Received: September 18, 2024
Revised: October 13, 2024
Accepted: October 15, 2024
Published: October 18, 2024

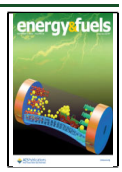

Downloaded via UNIV OF CALIFORNIA SANTA CRUZ on August 17, 2025 at 14:35:33 (UTC).
See https://pubs.acs.org/sharingguidelines for options on how to legitimately share published articles.

ACS Publications

© 2024 American Chemical Society

https://doi.org/10.1021/acs.energyfuels.4c04554
Energy Fuels 2024, 38, 21382–21387

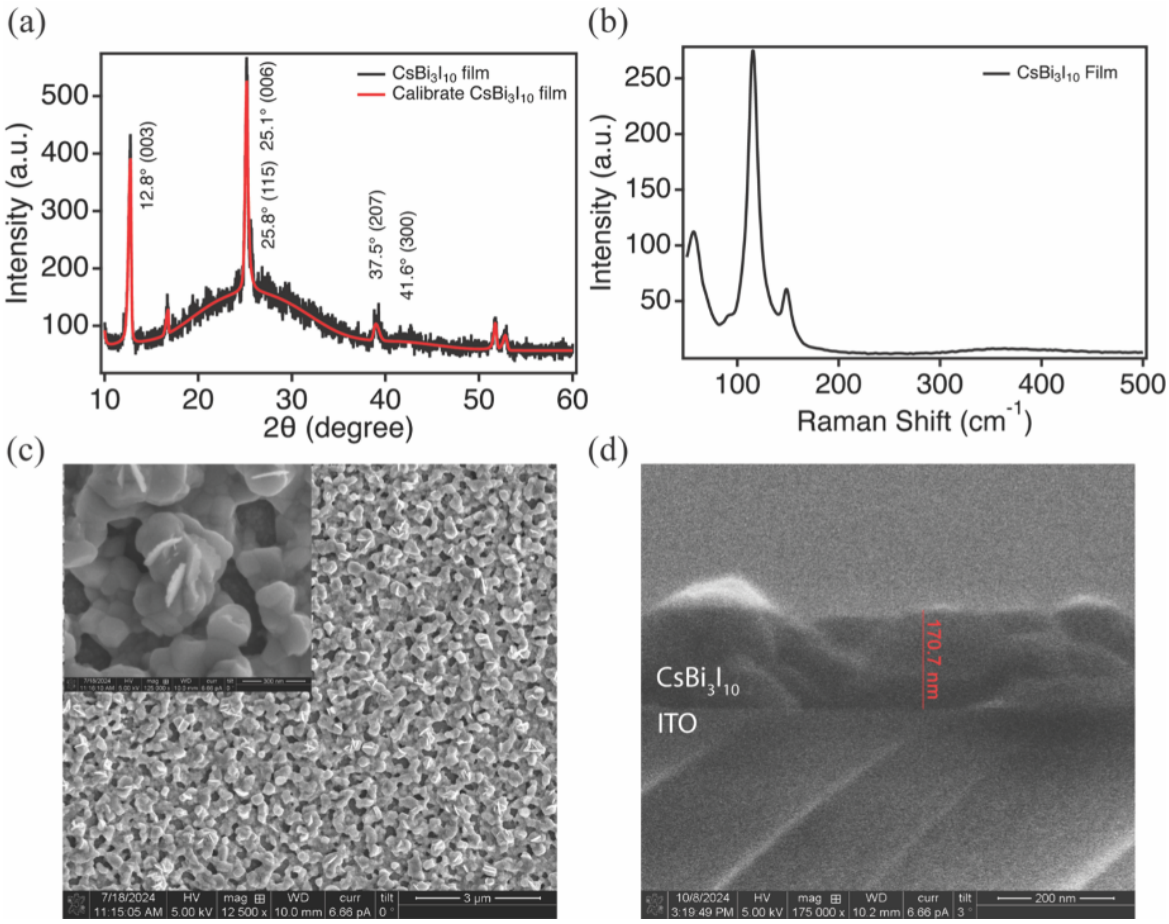

Figure 1. (a) XRD pattern of $CsBi_3I_{10}$, (b) Raman spectrum of $CsBi_3I_{10}$, (c) SEM images of the $CsBi_3I_{10}$ film (inset: higher magnitude), and (d) SEM cross-section of the $CsBi_3I_{10}$ film.

recombination, offering insights into improving light-harvesting efficiency.[31] Additionally, Ghimire et al. investigated quasi-two-dimensional $Cs_3Bi_2I_9$ nanosheets and found that the strong excitonic interactions and anisotropic charge transport within these nanosheets could be leveraged to develop more efficient solar cells.[32] By comparison, the dynamics of photoexcited charge carriers in Pb-free $CsBi_3I_{10}$ thin films has been scarcely investigated. A detailed exploration of exciton dynamics for $CsBi_3I_{10}$ perovskite films is crucial to enhancing our knowledge of the excited states within these materials and aiding in designing sustainable, hot carrier-based solar cells.

In this work, we synthesized $CsBi_3I_{10}$ perovskite films and examined their morphology and crystal structure using scanning electron microscopy (SEM) and X-ray diffraction (XRD). The $CsBi_3I_{10}$ perovskite films showed two excitonic peaks in ultraviolet−visible (UV−vis) absorption. Femtosecond transient absorption spectroscopy (TAS) was used to investigate the exciton dynamics in the $CsBi_3I_{10}$ perovskite films.

Figure 1a shows the XRD pattern of the $CsBi_3I_{10}$ thin film, which is consistent with previously reported result,[33] because the Joint Committee on Powder Diffraction Standards (JCPDS) card number for the reference pattern of $CsBi_3I_{10}$ is unavailable. $CsBi_3I_{10}$ reveals the most significant peaks at 12.8°, 25.1°, and 25.8° (2θ), which correspond to the (003), (006), and (115) planes, respectively.[33] The average grain size of the $CsBi_3I_{10}$ thin film was calculated to be 23.7 ± 0.7 nm using Scherrer's formula for the 12.8° and 25.1° peaks

$$D = \frac{K\lambda}{\beta \cos\theta} \quad (1)$$

where D is the average grain size, K is the Scherrer constant, λ is the X-ray wavelength, β is the half-width of the measured diffraction peak, and θ is the diffraction angle. In addition, Raman spectra of the $CsBi_3I_{10}$ thin film were measured to further assess crystal quality, as shown in Figure 1b, which exhibit characteristic peaks at 60, 116, and 146 cm^{-1}, consistent with that reported in previous theoretical and experimental studies.[34−36] The peak at 112 cm^{-1} (A_g),[35] characteristic of BiI_3, was also observed, indicating its presence in the thin film. Furthermore, SEM images reveal larger hexagonal grains of up to 200 nm and a thin-film thickness of approximately 170 nm on the indium tin oxide (ITO) substrate, as shown in panels c and d of Figure 1. The large particles observed by SEM are likely composed of smaller particles or domains with grain boundaries revealed by XRD. The grain boundaries along with the large surface-to-volume (S/V) ratio of nanoparticles in general tend to lead to a high density of defects. These defects likely result in trap states within the bandgap that can significantly affect optical properties and dynamics of charge carriers. This is consistent

https://doi.org/10.1021/acs.energyfuels.4c04554
Energy Fuels 2024, 38, 21382−21387

with the overall short lifetime observed in ultrafast dynamic studies and the non-detectable photoluminescence (PL), as discussed later.

Figure 2 shows the UV−vis electronic absorption spectra of $CsBi_3I_{10}$ thin films, where the first and second excitonic bands

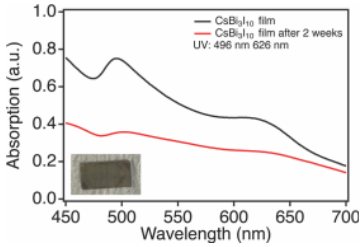

Figure 2. UV−vis electronic absorption spectra of $CsBi_3I_{10}$ thin films (inset: fresh thin-film optical photograph).

are peaked at 496 nm (2.45 eV) and 626 nm (1.98 eV), respectively, consistent with a previous report.[37] In addition, the calculated direct optical bandgap energy of the $CsBi_3I_{10}$ perovskite is around 1.77 eV,[38,39] which is usually smaller than the experimental value due to the PER-DFT calculations.[13] The inset of Figure 2 shows a photograph of the $CsBi_3I_{10}$ material on an ITO glass substrate, in a brown/black color after annealing. To determine if the two absorption bands are from the same $CsBi_3I_{10}$ species, we stored the $CsBi_3I_{10}$ thin films under an ambient atmosphere at 25 °C with 60% relative humidity and monitored their degradation over time with UV−vis spectroscopy for 2 weeks. The two bands degraded at a very similar rate, suggesting that both absorption bands originate from $CsBi_3I_{10}$.

The femtosecond TAS spectra of the as-prepared $CsBi_3I_{10}$ samples were measured using either a 470 or 580 nm pump and white-light probe (520−750 nm) as a function of the time delay between the pump and probe pulses to determine the exciton dynamics. To avoid nonlinear processes, such as Auger recombination or exciton−exciton annihilation, each sample was pumped with multiple pulse energies (25, 50, 65, and 85 nJ/pulse) to investigate linear power regions in the recombination dynamics,[40] as shown in Figure S1 of the Supporting Information. The TA/TB results with excitation at 470 and 580 nm show no indication of nonlinear dynamics in the 25−85 nJ/pulse region.

Figure 3a shows the TA/TB spectra of $CsBi_3I_{10}$ thin films with 470 nm excitation and different time delays. The three observed features are a weak transient absorption (TA_1, excited-state absorption) at 574 nm, followed by the sharp transient bleach (TB, ground-state depletion) at 623 nm and sharp transient absorption (TA_2) at 663 nm. Here, the TB signal (623 nm) is consistent with a similar absorption peak (626 nm) observed in the UV−vis absorption spectra, as expected.

Panels b and c of Figure 3 show the TB and TA_2 kinetic profiles of the $CsBi_3I_{10}$ thin film collected under the second lowest pump power (50 nJ/pulse) with excitation at 470 nm. The TB recovery feature of $CsBi_3I_{10}$ can be fit to a triple exponential decay function with time constants of 0.27 ± 0.06, 2.7 ± 1.1, and 582 ± 240 ps (Table 1). The fitting functions and related parameters are discussed in the Supporting Information.[41,42] The fast recovery component has a dominant amplitude of 83% and is likely the result of the hot electron relaxation in the conduction band (CB) to the conduction

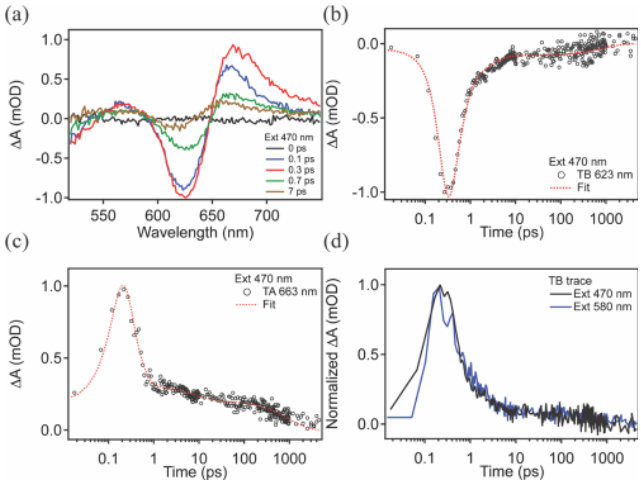

Figure 3. (a) Difference in absorption spectrum as a function of the wavelength and varying probe delay time, (b) TB and (c) TA_2 signal profiles and fits of a $CsBi_3I_{10}$ thin film, and (d) overlaid normalized transient bleach recovery with excitation at 470 and 580 nm with similar power.

band edge (CB_{edge}), while the intermediate recovery with 11% amplitude may be attributed to the trapping of electrons from the CB_{edge} to the trap states (TSs). Last, the slow recovery with 6% amplitude is assigned to TS to valence band (VB) recombination. Similar to observations in $PbBr_2$ molecular clusters[43] by Zhang et al., the short lifetime in $CsBi_3I_{10}$ may be influenced by dissociative excited states that lead to rapid non-radiative decay and possibly photoinduced degradation. A comparison between the TB results measured under the linear pump power (50 nJ/pulse) with 470 and 580 nm excitation is shown in Figure 3d. The extracted kinetic profiles show similar dynamics regardless of the excitation wavelength, suggesting that the 470 nm excitation likely promotes electrons to the second excitonic state that then rapidly relaxes to the first excitonic state. Although the spectra show two TA kinetic decay features, TA_1 shows a lower signal-to-noise (S/N) ratio due to the inference between the pump and probe beams. Because of this, we analyze only the TA_2 decay for this study. The TA_2 decays can be fit with a triple exponential function with similar fast, medium, and slow constants of 0.20 ± 0.05, 4.9 ± 1.1, and 698 ± 250 ps (Table 1) as the TB signal. The similar kinetics of the TB and TA_2 signals suggest that they are associated with similar processes.

To gain further insight into the physical processes governing the exciton and charge carrier dynamics in the present thin film, we proposed a kinetic model, as shown in Figure S2a of the Supporting Information, to fit the observed TB and TA_2 signals, following an approach similar to previous studies.[44−48] The proposed model for pristine $CsBi_3I_{10}$ involves the CB, CB_{edge}, TS, and VB. The rate constant for each transition is iterative and selected on the basis of the best fit to the experimental results, as shown in the Supporting Information. In this proposed model, we assign the time constants to the corresponding physical processes in the $CsBi_3I_{10}$ samples (Table S1 of the Supporting Information). This kinetic modeling is not unique, but it does provide a possible scenario to better understand the key dynamic processes involved. On the basis of the results of TB, TA_2, and related kinetic modeling, possible mechanisms are proposed to explain the exciton dynamics in the $CsBi_3I_{10}$ thin film in Figure 4.

https://doi.org/10.1021/acs.energyfuels.4c04554
Energy Fuels 2024, 38, 21382−21387

Table 1. Fitting Parameters of Single-Wavelength TB Recovery at λ_{max} of the $CsBi_3I_{10}$ Thin Film

$CsBi_3I_{10}$	τ_1 (ps)	τ_2 (ps)	τ_3 (ps)	A_1	A_2	A_3
TB, 623 nm	0.27 ± 0.06	2.7 ± 1.1	582 ± 240	−1.5 ± 0.1 (78%)	−0.3 ± 0.1 (15%)	−0.1 ± 0.05 (7%)
TA, 663 nm	0.20 ± 0.05	4.9 ± 1.1	698 ± 250	1.2 ± 0.1 (80%)	0.1 ± 0.1 (7%)	0.2 ± 0.05 (13%)

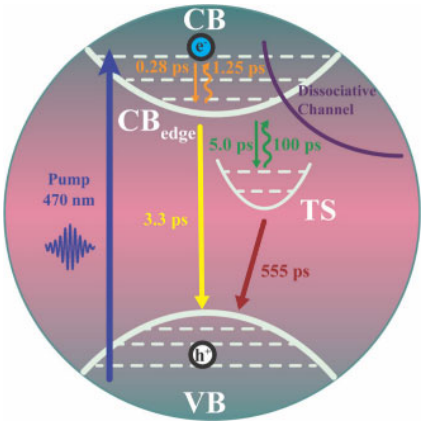

Figure 4. Kinetic model of $CsBi_3I_{10}$. The lifetimes of each state were calculated using the kinetic model of the TB and TA results.

Following excitation with an energy above the band gap (470 nm), an exciton is generated. Exciting above the band edge provides excess kinetic energy, and therefore, the electron will relax to the CB_{edge} through electron−phonon interactions.[49] In $CsBi_3I_{10}$, the fast component (~0.28 ps) in the TB recovery and TA_2 decay profile was attributed to vibrational relaxation or cooling of the excitons within the CB, potentially influenced by defects due to surface and grain boundaries. After the electrons relax to the CB_{edge}, they can relax through multiple pathways, including trapping into trap states. The presence of surface defects is expected to enhance charge carrier trapping, as also discussed in previous studies on similar materials.[50−52] In the simplified model, the TB and TA_2 medium component (~5 ps) was attributed to trapping below the CB_{edge}. Moreover, the modeling suggests that the electron−hole recombination process has contributions from the TS. Specifically, the slow components from the TB and TA_2 data show that recombination from the TS to VB occurs in ~555 ps. This slow recombination from the TS to VB might be due to free carriers forming polarons highly localized in the TS.[53] Interestingly, from the kinetic fitting model, band-to-band recombination was suggested to be ~3.3 ps. A possible explanation for this phenomenon is due to an excited state coupled with a dissociative channel, which can impact the overall exciton dynamic.[43] The dissociative excited state offers a non-radiative decay pathway, allowing excitons to rapidly dissociate rather than undergoing radiative recombination. The presence of such a dissociative channel not only shortens the excited state lifetime but also competes with other relaxation pathways, such as electron trapping in TS and electron−hole recombination from the CB_{edge} to the VB. It also likely leads to photoinduced degradation of the material.

Furthermore, the triple exponential decay observed in the TB and TA_2 signals indicates that the dynamic processes involved are not solely sequential or parallel but also involve multiple and reverse processes. The reverse processes, represented as upward-curved arrows in Figure 4, are generally expected to be slower than the forward processes and likely result from back energy transfer from a vibrationally relaxed state, such as the CB_{edge} or TS, to higher vibrational states, contributing to the multiexponential behavior. Specifically, reverse processes with time constants of 1.25 and 100 ps were identified. The faster reverse process (1.25 ps) likely corresponds to back transfer from the vibrationally relaxed states to higher energy states, while the slower reverse process (100 ps) might be attributed to a delayed backflow from trapped states. The rate constants and corresponding time constants for each process are detailed in Table S1 of the Supporting Information. In the kinetic model, various combinations of rate and time constants were simulated to determine the most likely processes occurring within the $CsBi_3I_{10}$ system, with details given in the Supporting Information.

In summary, the exciton dynamics of the $CsBi_3I_{10}$ thin film have been investigated for the first time using femtosecond TA spectroscopy. The $CsBi_3I_{10}$ thin film was synthesized by the antisolvent spin-coating technique, and the crystallinity was confirmed using XRD and Raman measurements. Furthermore, UV−vis absorption spectra revealed two excitonic peaks peaked at 496 and 626 nm. Detailed kinetic analysis of ultrafast TB and TA dynamics suggests hot electron cooling in the conduction band, trapping in trap states, electron−hole recombination, and possible involvement of a dissociative pathway or high density of defect states coupled with the excited electronic state, leading to overall short-lived exciton or charge carriers. These results are important for gaining a deeper understanding of the photophysics of Bi-based halide perovskites and represent an important first step toward improving their performance.

■ ASSOCIATED CONTENT

Supporting Information

The Supporting Information is available free of charge at https://pubs.acs.org/doi/10.1021/acs.energyfuels.4c04554.

Details of the experimental section, material characterization (UV−vis absorption, XRD, and SEM), femtosecond TAS measurements, fitting parameters of the TAS results, and details regarding the kinetic modeling of charge-carrier dynamics (PDF)

■ AUTHOR INFORMATION

Corresponding Author

Jin Z. Zhang − *Department of Chemistry and Biochemistry, University of California, Santa Cruz, Santa Cruz, California 95064, United States;* orcid.org/0000-0003-3437-912X; Phone: +1-831-459-3776; Email: zhang@ucsc.edu

Authors

Kai-Chun Chou − *Department of Chemistry and Biochemistry, University of California, Santa Cruz, Santa Cruz, California 95064, United States;* orcid.org/0000-0002-0282-3604

David C. Zeitz − *Department of Chemistry and Biochemistry, University of California, Santa Cruz, Santa Cruz, California 95064, United States;* orcid.org/0009-0006-0473-1849

Mariam Khvichia − *Department of Chemistry and Biochemistry, University of California, Santa Cruz, Santa Cruz, California 95064, United States*

Jeremy L. Barnett − *Department of Chemistry and Biochemistry, University of California, Santa Cruz, Santa Cruz, California 95064, United States;* orcid.org/0000-0003-3483-847X

Complete contact information is available at: https://pubs.acs.org/10.1021/acs.energyfuels.4c04554

Notes

The authors declare no competing financial interest.

■ ACKNOWLEDGMENTS

The authors are grateful to the U.S. National Science Foundation (NSF) for financial support (CHE-2203633). SEM imaging was conducted with the assistance of Dr. Tom Yuzvinsky at the W. M. Keck Center for Nanoscale Optofluidic on the FEI Quanta 3D dualbeam microscope.

■ REFERENCES

(1) Sim, K.; Jun, T.; Bang, J.; Kamioka, H.; Kim, J.; Hiramatsu, H.; Hosono, H. Performance Boosting Strategy for Perovskite Light-Emitting Diodes. *Appl. Phys. Rev.* **2019**, *6* (3), 031402.

(2) Steele, J. A.; Pan, W.; Martin, C.; Keshavarz, M.; Debroye, E.; Yuan, H.; Banerjee, S.; Fron, E.; Jonckheere, D.; Kim, C. W.; Baekelant, W.; Niu, G.; Tang, J.; Vanacken, J.; Van der Auweraer, M.; Hofkens, J.; Roeffaers, M. B. J. Photophysical Pathways in Highly Sensitive $Cs_2AgBiBr_6$ Double-Perovskite Single-Crystal X-ray Detectors. *Adv. Mater.* **2018**, *30* (46), 1804450.

(3) Xing, G.; Mathews, N.; Lim, S. S.; Yantara, N.; Liu, X.; Sabba, D.; Grätzel, M.; Mhaisalkar, S.; Sum, T. C. Low-Temperature Solution-Processed Wavelength-Tunable Perovskites for Lasing. *Nat. Mater.* **2014**, *13* (5), 476−480.

(4) Fang, Y.; Dong, Q.; Shao, Y.; Yuan, Y.; Huang, J. Highly Narrowband Perovskite Single-Crystal Photodetectors Enabled by Surface-Charge Recombination. *Nat. Photonics* **2015**, *9* (10), 679−686.

(5) Lian, Z.; Yan, Q.; Gao, T.; Ding, J.; Lv, Q.; Ning, C.; Li, Q.; Sun, J. Perovskite $CH_3NH_3PbI_3(Cl)$ Single Crystals: Rapid Solution Growth, Unparalleled Crystalline Quality, and Low Trap Density toward 108 cm^{-3}. *J. Am. Chem. Soc.* **2016**, *138* (30), 9409−9412.

(6) Quan, L. N.; Rand, B. P.; Friend, R. H.; Mhaisalkar, S. G.; Lee, T.-W.; Sargent, E. H. Perovskites for Next-Generation Optical Sources. *Chem. Rev.* **2019**, *119* (12), 7444−7477.

(7) Ponti, C.; Nasti, G.; Di Girolamo, D.; Cantone, I.; Alharthi, F. A.; Abate, A. Environmental Lead Exposure from Halide Perovskites in Solar Cells. *Trends Ecol. Evol.* **2022**, *37* (4), 281−283.

(8) Li, J.; Duan, J.; Yang, X.; Duan, Y.; Yang, P.; Tang, Q. Review on Recent Progress of Lead-Free Halide Perovskites in Optoelectronic Applications. *Nano Energy* **2021**, *80*, 105526.

(9) Wu, C.; Zhang, Q.; Liu, G.; Zhang, Z.; Wang, D.; Qu, B.; Chen, Z.; Xiao, L. From Pb to Bi: A Promising Family of Pb-Free Optoelectronic Materials and Devices. *Adv. Energy Mater.* **2020**, *10* (13), 1902496.

(10) Yang, J.; Bao, C.; Ning, W.; Wu, B.; Ji, F.; Yan, Z.; Tao, Y.; Liu, J.-M.; Sum, T. C.; Bai, S.; Wang, J.; Huang, W.; Zhang, W.; Gao, F. Stable, High-Sensitivity and Fast-Response Photodetectors Based on Lead-Free $Cs_2AgBiBr_6$ Double Perovskite Films. *Adv. Opt. Mater.* **2019**, *7* (13), 1801732.

(11) Min, H.; Chang, J.; Tong, Y.; Wang, J.; Zhang, F.; Feng, Z.; Bi, X.; Chen, N.; Kuang, Z.; Wang, S.; Yuan, L.; Shi, H.; Zhao, N.; Qian, D.; Xu, S.; Zhu, L.; Wang, N.; Huang, W.; Wang, J. Additive Treatment Yields High-Performance Lead-Free Perovskite Light-Emitting Diodes. *Nat. Photonics* **2023**, *17* (9), 755−760.

(12) Liu, C.-K.; Tai, Q.; Wang, N.; Tang, G.; Loi, H.-L.; Yan, F. Sn-Based Perovskite for Highly Sensitive Photodetectors. *Adv. Sci.* **2019**, *6* (17), 1900751.

(13) Krishnamoorthy, T.; Ding, H.; Yan, C.; Leong, W. L.; Baikie, T.; Zhang, Z.; Sherburne, M.; Li, S.; Asta, M.; Mathews, N.; Mhaisalkar, S. G. Lead-Free Germanium Iodide Perovskite Materials for Photovoltaic Applications. *J. Mater. Chem. A* **2015**, *3* (47), 23829−23832.

(14) Zeng, H.; Yao, F.; Li, R.; Song, D.; Li, Y.; Lin, Q.; Xie, R.-J. Thermal Evaporation of Lead-Free Inorganic Perovskite $CsGeI_3$ for Photodetection. *Appl. Phys. Lett.* **2022**, *121* (10), 101101.

(15) Xie, L.; Chen, B.; Zhang, F.; Zhao, Z.; Wang, X.; Shi, L.; Liu, Y.; Huang, L.; Liu, R.; Zou, B.; Wang, Y. Highly Luminescent and Stable Lead-Free Cesium Copper Halide Perovskite Powders for UV-Pumped Phosphor-Converted Light-Emitting Diodes. *Photonics Res.* **2020**, *8* (6), 768−775.

(16) Cui, W.; Zhao, J.; Wang, L.; Lv, P.; Li, X.; Yin, Z.; Yang, C.; Tang, A. Unraveling the Phase Transition and Luminescence Tuning of Pb-Free Cs−Cu−I Perovskites Enabled by Reaction Temperature and Polar Solvent. *J. Phys. Chem. Lett.* **2022**, *13* (22), 4856−4863.

(17) Li, S.; He, J.; Ran, R.; Zhou, W.; Wang, W.; Shao, Z. Lead-Free All-Inorganic Cesium Bismuth Iodide-Based Perovskite Solar Cells: Recent Advances, Current Limitations, and Future Prospects. *Sol. RRL* **2024**, *8* (5), 2300984.

(18) Kumar Chini, M.; Goverapet Srinivasan, S.; Tailor, N. K.; Yukta; Salahub, D.; Satapathi, S. Lead-Free, Stable Mixed Halide Double Perovskites $Cs_2AgBiBr_6$ and $Cs_2AgBiBr_{6-x}Cl_x$—A Detailed Theoretical and Experimental Study. *Chem. Phys.* **2020**, *529*, 110547.

(19) Qi, Z.; Fu, X.; Yang, T.; Li, D.; Fan, P.; Li, H.; Jiang, F.; Li, L.; Luo, Z.; Zhuang, X.; Pan, A. Highly Stable Lead-Free $Cs_3Bi_2I_9$ Perovskite Nanoplates for Photodetection Applications. *Nano Res.* **2019**, *12* (8), 1894−1899.

(20) Xiong, Z.; Hu, W.; She, Y.; Lin, Q.; Hu, L.; Tang, X.; Sun, K. Air-Stable Lead-Free Perovskite Thin Film Based on $CsBi_3I_{10}$ and Its Application in Resistive Switching Devices. *ACS Appl. Mater. Interfaces* **2019**, *11* (33), 30037−30044.

(21) Liu, R.; Zhou, H.; Wang, R.; Wu, D.; Pan, X.; Pan, G.; Wang, H. Space-Confined Growth of High-Quality $CsBi_3I_{10}$ Lead-Free Perovskite Film for Near-Infrared Photodetectors with High Sensitivity and Stability. *Sci. China Mater.* **2021**, *64* (2), 393−399.

(22) Singh, T.; Kulkarni, A.; Ikegami, M.; Miyasaka, T. Effect of Electron Transporting Layer on Bismuth-Based Lead-Free Perovskite $(CH_3NH_3)_3Bi_2I_9$ for Photovoltaic Applications. *ACS Appl. Mater. Interfaces* **2016**, *8* (23), 14542−14547.

(23) Tailor, N. K.; Mishra, S.; Sharma, T.; De, A. K.; Satapathi, S. Cation-Dependent Hot Carrier Cooling in the Lead-Free Bismuth Halide $A_3Bi_2I_9$ (A = FA, MA, and Cs) Perovskite. *J. Phys. Chem. C* **2021**, *125* (18), 9891−9898.

(24) Wenderott, J. K.; Raghav, A.; Shtein, M.; Green, P. F.; Satapathi, S. Local Optoelectronic Characterization of Solvent-Annealed, Lead-Free, Bismuth-Based Perovskite Films. *Langmuir* **2018**, *34* (26), 7647−7654.

(25) Lyu, M.; Yun, J.-H.; Cai, M.; Jiao, Y.; Bernhardt, P. V.; Zhang, M.; Wang, Q.; Du, A.; Wang, H.; Liu, G.; Wang, L. Organic−Inorganic Bismuth(III)-Based Material: A Lead-Free, Air-Stable and Solution-Processable Light-Absorber beyond Organolead Perovskites. *Nano Res.* **2016**, *9* (3), 692−702.

(26) Sebastia-Luna, P.; Gélvez-Rueda, M. C.; Dreessen, C.; Sessolo, M.; Grozema, F. C.; Palazon, F.; Bolink, H. J. Potential and Limitations of $CsBi_3I_{10}$ as a Photovoltaic Material. *J. Mater. Chem. A* **2020**, *8* (31), 15670−15674.

(27) Shin, J.; Kim, M.; Jung, S.; Kim, C. S.; Park, J.; Song, A.; Chung, K.-B.; Jin, S.-H.; Lee, J. H.; Song, M. Enhanced Efficiency in Lead-Free Bismuth Iodide with Post Treatment Based on a Hole-Conductor-Free Perovskite Solar Cell. *Nano Res.* **2018**, *11* (12), 6283−6293.

(28) Park, B.-W.; Philippe, B.; Zhang, X.; Rensmo, H.; Boschloo, G.; Johansson, E. M. J. Bismuth Based Hybrid Perovskites $A_3Bi_2I_9$ (A:

Methylammonium or Cesium) for Solar Cell Application. *Adv. Mater.* **2015**, *27* (43), 6806−6813.
(29) Vijaya, S.; Subbiah, J.; Jones, D. J.; Anandan, S. LARP-Assisted Synthesis of $CsBi_3I_{10}$ Perovskite for Efficient Lead-Free Solar Cells. *RSC Adv.* **2023**, *13* (15), 9978−9982.
(30) Igbari, F.; Wang, R.; Wang, Z.-K.; Ma, X.-J.; Wang, Q.; Wang, K.-L.; Zhang, Y.; Liao, L.-S.; Yang, Y. Composition Stoichiometry of $Cs_2AgBiBr_6$ Films for Highly Efficient Lead-Free Perovskite Solar Cells. *Nano Lett.* **2019**, *19* (3), 2066−2073.
(31) Scholz, M.; Flender, O.; Oum, K.; Lenzer, T. Pronounced Exciton Dynamics in the Vacancy-Ordered Bismuth Halide Perovskite $(CH_3NH_3)_3Bi_2I_9$ Observed by Ultrafast UV−Vis−NIR Transient Absorption Spectroscopy. *J. Phys. Chem. C* **2017**, *121* (22), 12110−12116.
(32) Ghimire, S.; Rehhagen, C.; Fiedler, S.; Parekh, U.; Lesyuk, R.; Lochbrunner, S.; Klinke, C. Synthesis, Optoelectronic Properties, and Charge Carrier Dynamics of Colloidal Quasi-Two-Dimensional $Cs_3Bi_2I_9$ Perovskite Nanosheets. *Nanoscale* **2023**, *15* (5), 2096−2105.
(33) Johansson, M. B.; Zhu, H.; Johansson, E. M. J. Extended Photo-Conversion Spectrum in Low-Toxic Bismuth Halide Perovskite Solar Cells. *J. Phys. Chem. Lett.* **2016**, *7* (17), 3467−3471.
(34) Nilă, A.; Baibarac, M.; Matea, A.; Mitran, R.; Baltog, I. Exciton-Phonon Interactions in the $Cs_3Bi_2I_9$ Crystal Structure Revealed by Raman Spectroscopic Studies. *Phys. Status Solidi B* **2017**, *254* (4), 1552805.
(35) Saitoh, A.; Komatsu, T.; Karasawa, T.; Ohtake, H.; Suemoto, T. Raman Scattering under Hydrostatic Pressures in Layered BiI_3 and SbI_3 Crystals. *Phys. Status Solidi B* **2001**, *226* (2), 357−367.
(36) Tiwari, D.; Alibhai, D.; Fermin, D. J. Above 600 mV Open-Circuit Voltage BiI_3 Solar Cells. *ACS Energy Lett.* **2018**, *3* (8), 1882−1886.
(37) Khadka, D. B.; Shirai, Y.; Yanagida, M.; Miyano, K. Tailoring the Film Morphology and Interface Band Offset of Caesium Bismuth Iodide-Based Pb-Free Perovskite Solar Cells. *J. Mater. Chem. C* **2019**, *7* (27), 8335−8343.
(38) Wei, Z.; Ding, L.; Sun, N.; Dang, L.-Y.; Sun, H.-R.; Han, J.-C.; Zhu, J.-Q.; Wang, G.-G. Lead-Free $CsBi_3I_{10}$ Perovskite Based Photo-Enhanced Triboelectric Nanogenerator. *Nano Energy* **2023**, *108*, 108209.
(39) Liang, G.-X.; Chen, X.-Y.; Chen, Z.-H.; Lan, H.-B.; Zheng, Z.-H.; Fan, P.; Tian, X.-Q.; Duan, J.-Y.; Wei, Y.-D.; Su, Z.-H. Inorganic and Pb-Free $CsBi_3I_{10}$ Thin Film for Photovoltaic Applications. *J. Phys. Chem. C* **2019**, *123* (45), 27423−27428.
(40) Roberti, T. W.; Cherepy, N. J.; Zhang, J. Z. Nature of the Power-Dependent Ultrafast Relaxation Process of Photoexcited Charge Carriers in II−VI Semiconductor Quantum Dots: Effects of Particle Size, Surface, and Electronic Structure. *J. Chem. Phys.* **1998**, *108* (5), 2143−2151.
(41) Bodunov, E. N.; Antonov, Yu. A.; Simões Gamboa, A. L. On the Origin of Stretched Exponential (Kohlrausch) Relaxation Kinetics in the Room Temperature Luminescence Decay of Colloidal Quantum Dots. *J. Chem. Phys.* **2017**, *146* (11), 114102.
(42) Simões Gamboa, A. L.; Bodunov, E. N. Functions for Describing Nonexponential Photoluminescence Decay Kinetics in Semiconductor Nanocrystals. *Proceedings of the 2022 International Conference Laser Optics (ICLO)*; Saint Petersburg, Russian Federation, June 20−24, 2022; DOI: 10.1109/ICLO54117.2022.9839822.
(43) Zhang, H.; Zeitz, D. C.; Zhang, J. Z. Ultrafast Study of Excited State Dynamics of Amino Metal Halide Molecular Clusters. *J. Phys. Chem. Lett.* **2023**, *14* (36), 8095−8099.
(44) Cherrette, V. L.; Chou, K.-C.; Zeitz, D.; Guarino-Hotz, M.; Khvichia, M.; Barnett, J.; Win, A.; Babbe, F.; Zhang, J. Z. Ultrafast Exciton Dynamics of $CH_3NH_3PbBr_3$ Perovskite Nanoclusters. *J. Phys. Chem. Lett.* **2024**, *15* (19), 5177−5182.
(45) Pu, Y.-C.; Kibria, M. G.; Mi, Z.; Zhang, J. Z. Ultrafast Exciton Dynamics in InGaN/GaN and Rh/Cr_2O_3 Nanoparticle-Decorated InGaN/GaN Nanowires. *J. Phys. Chem. Lett.* **2015**, *6* (13), 2649−2656.
(46) Chou, K.-C.; Li, L.-C.; Tsai, K.-A.; Zeitz, D. C.; Pu, Y.-C.; Zhang, J. Z. Effect of Lattice Disorder on Exciton Dynamics in Copper-Doped $InP/ZnSe_xS_{1-x}$ Core/Shell Quantum Dots. *J. Phys. Chem. Lett.* **2024**, *15* (16), 4311−4318.
(47) Wu, J.; Li, X.; Lian, X.; Su, B.; Pang, J.; Li, M.-D.; Xia, Z.; Zhang, J. Z.; Luo, B.; Huang, X.-C. Ultrafast Study of Exciton Transfer in Sb(III)-Doped Two-Dimensional $[NH_3(CH_2)_4NH_3]CdBr_4$ Perovskite. *ACS Nano* **2021**, *15* (9), 15354−15361.
(48) Khvichia, M.; Chou, K.-C.; Lee, S.; Zeitz, D. C.; Zou, S.; Li, Y.; Zhang, J. Z. Ultrafast Photoinduced Charge Carrier Dynamics of L-Cysteine and Oleylamine Stabilized $CsPbBr_3$ Perovskite Quantum Dots Coupled with Gold Nanoparticles. *J. Chem. Phys.* **2024**, *161* (11), 114704.
(49) Fu, J.; Xu, Q.; Han, G.; Wu, B.; Huan, C. H. A.; Leek, M. L.; Sum, T. C. Hot Carrier Cooling Mechanisms in Halide Perovskites. *Nat. Commun.* **2017**, *8* (1), 1300.
(50) Zheng, K.; Žídek, K.; Abdellah, M.; Chen, J.; Chábera, P.; Zhang, W.; Al-Marri, M. J.; Pullerits, T. High Excitation Intensity Opens a New Trapping Channel in Organic−Inorganic Hybrid Perovskite Nanoparticles. *ACS Energy Lett.* **2016**, *1* (6), 1154−1161.
(51) Mondal, N.; Samanta, A. Complete Ultrafast Charge Carrier Dynamics in Photo-Excited All-Inorganic Perovskite Nanocrystals ($CsPbX_3$). *Nanoscale* **2017**, *9* (5), 1878−1885.
(52) Bodunov, E. N.; Simões Gamboa, A. L. Photoluminescence Decay of Colloidal Quantum Dots: Reversible Trapping and the Nature of the Relevant Trap States. *J. Phys. Chem. C* **2019**, *123* (41), 25515−25523.
(53) Wu, B.; Ning, W.; Xu, Q.; Manjappa, M.; Feng, M.; Ye, S.; Fu, J.; Lie, S.; Yin, T.; Wang, F.; Goh, T. W.; Harikesh, P. C.; Tay, Y. K. E.; Shen, Z. X.; Huang, F.; Singh, R.; Zhou, G.; Gao, F.; Sum, T. C. Strong Self-Trapping by Deformation Potential Limits Photovoltaic Performance in Bismuth Double Perovskite. *Sci. Adv.* **2021**, *7* (8), eabd3160.